Multiphysics response of magneto-electro-elastic beams in thermo-mechanical environment

Vinyas M. and S.C. Kattimani[*]

Department of Mechanical Engineering, National Institute of Technology Karnataka, Surathkal, 575025, India

Abstract.   In this article, the multiphysics response of magneto-electro-elastic (MEE) cantilever beam subjected to thermo-mechanical loading is analysed. The equilibrium equations of the system are obtained with the aid of the principle of total potential energy. The constitutive equations of a MEE material accounting the thermal fields are used for analysis. The corresponding finite element (FE) formulation is derived and model of the beam is generated using an eight noded 3D brick element. The 3D FE formulation developed enables the representation of governing equations in all three axes, achieving accurate results. Also, geometric, constitutive and loading assumptions required to dimensionality reduction can be avoided. Numerical evaluation is performed on the basis of the derived formulation and the influence of various mechanical loading profiles and volume fractions on the direct quantities and stresses is evaluated. In addition, an attempt has been made to compare the individual effect of thermal and mechanical loading with the combined effect. It is believed that the numerical results obtained helps in accurate design and development of sensors and actuators.

Keywords: finite element; magneto-electro-elastic beam; thermo-mechanical load; direct quantities; volume fraction

1. Introduction

   The looming technologies along with the advancement in the production and application of the composite materials have paved way for the new class of materials know as smart materials, among which the particular interest is vested on the magneto-electro-elastic (MEE) materials which are made of both piezoelectric and piezomagnetic phases. In the last decade, ample amount of research has been carried out on analysing the structural behavior of MEE structures like plates, beams and shells. Pan and Han (2005) presented an exact solution for the layered functionally graded (FG) MEE rectangular plate. Kattimani and Ray (2014a, b) explored the active control of geometrically nonlinear vibrations of MEE plates and doubly curved shells. They also examined the same for the functionally graded MEE plates (2015). Bhangale and Ganeshan (2006) evaluated the free vibration analysis of functionally graded MEE plates using a semi analytical finite element

─────────────

∗Corresponding author, E-mail: sck@nitk.ac.in

(FE) model. A FE model developed by Annigeri *et al.* (2007) assists to investigate the free vibrations of multiphase and layer-wise MEE beam. Milazzo *et al.* (2013) derived an analytical solution to compute the free and forced vibration behavior of MEE bi-morph beam. This method proved its effectiveness for both multiphase and laminated beam structures. Biju *et al.* (2012a, b) discussed the behavior of a MEE sensor patch mounted on the steel beam under harmonic loading. They figured out the effect of patch location and different boundary conditions on the transient dynamic response of the beam. In addition, the response of MEE beam when applied with time harmonic electric potential has been studied. Vaezi *et al.* (2016) demonstrated the effect of the electric and magnetic potentials on the stiffness and stability of the MEE microbeams. The FE model of the fully coupled thermopiezomagnetic continuum derived by Sunar *et al.* (2002) gave rise to a plentiful research work on the thermal analysis of the MEE structures. Ebrahimi and Barati (2016) investigated the thermal vibrations of the magneto-thermo-electro-elastic (MTEE) nano beams. Using the Eringen's nonlocal elasticity theory and Hamilton's principle, the nonlocal nonlinear governing equations of a nano beams subjected to thermo-electro- magneto loads were presented by Ansari *et al.* (2015). Jandaghian and Rahmani (2016) studied the free vibration analysis of MTEE beams resting on Pasternak foundation by using nonlocal and Timoshenko beam theory. They found that natural frequency is insensitive to temperature changes. Kumaravel *et al.* (2007) investigated the static behavior of the MEE strip in thermal environment. Kondaiah *et al.* (2012 a, b) considered the pyroeffects and evaluated the behavior of the MEE beams and plates subjected to uniform temperature using the FE formulation. Ootao and Tanigawa (2005) developed an exact solution for the transient behavior of multilayered MTEE strip subjected to non-uniform and unsteady heating. Kim *et al.* (2012) derived an analytical expression to analyze the product properties of FG transversely isotropic MTEE multilayer composite with an arbitrary number of layers. Badri and Kayiem (2013) used the first order shear deformation theory (FSDT) to study the static and dynamic analysis of MTEE plates. More recently, Vinyas and Kattimani (2017a, b) developed a FE formulation and analyzed the thermal response of MEE beam and plates. They extended their evaluation for multiphase MEE beams subjected to different temperature loading also (Vinyas and Kattimani 2017c).

In this article, the 3D equilibrium equation for the static analysis of MEE structure subjected to various loads (thermal, mechanical, electric and magnetic loads) is derived considering the simple total potential energy and constitutive equations. Also, from the literature survey it is observed that the work carried out on the analysis of the MEE structure subjected to the thermo-mechanical loading is available in scarce. In particular, no literature has been reported on finite element formulation of MEE structures subjected to thermal and mechanical load together. Hence, in this article an attempt has been made to investigate the static response of the MEE beam subjected to combination of thermal and mechanical loads. It is believed that the present study helps in the design, analysis and development of the sensors and actuators.

2. Problem description

2.1 Beam geometry

The schematic representation of the cantilever MEE beam is depicted in Fig. 1. The beam length L is taken along the x-axis of the Cartesian co-ordinate. The thickness h and width b of the beam are measured along z and y directions, respectively. The boundary conditions incorporated at the clamped end are $u = v = w = \phi = \psi = 0$.
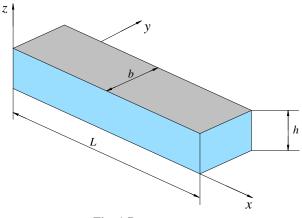
Fig. 1 Beam geometry

Table 1 Material properties of BaTiO$_3$-CoFe$_2$O$_4$ composite w.r.t different volume fraction V_f of BaTiO$_3$ (Kondaiah *et al.* 2012)

Material property	Material constants	0.0 V_f	0.2 V_f	0.4 V_f	0.5 V_f	0.6 V_f	0.8 V_f	1 V_f
Elastic constants (GPa)	$C_{11}=C_{22}$	286	250	225	220	200	175	166
	C_{12}	173	146	125	120	110	100	77
	$C_{13}=C_{23}$	170	145	125	120	110	100	78
	C_{33}	269.5	240	220	215	190	170	162
	$C_{44}=C_{55}$	45.3	45	45	45	45	50	43
	C_{66}	56.5	52	50	50	45	37.5	44.5
Piezoelectric constants (C/m^2)	e_{31}	0	-2	-3	-3.5	-3.5	-4	-4.4
	e_{33}	0	4	7	9.0	11	14	18.6
	e_{15}	0	0	0	0	0	0	11.6
Dielectric constant (10^{-9} C^2/Nm^2)	$\varepsilon_{11}=\varepsilon_{22}$	0.08	0.33	0.8	0.85	0.9	1	11.2
	ε_{33}	0.093	2.5	5	6.3	7.5	10	12.6
Magnetic permeability (10^{-4} Ns^2/C^2)	$\mu_{11}=\mu_{22}$	-5.9	-3.9	-2.5	-2.0	-1.5	-0.8	0.05
	μ_{33}	1.57	1.33	1	0.9	0.75	0.5	0.1
Piezomagnetic constants (N/Am)	q_{31}	580	410	300	350	200	100	0
	q_{33}	700	550	380	320	260	120	0
	q_{15}	560	340	220	200	180	80	0
Magneto-electric constant (10^{-12} Ns/VC)	$m_{11}=m_{22}$	0	2.8	4.8	5.5	6	6.8	0
	m_{33}	0	2000	2750	2600	2500	1500	0
Pyroelectric constant (10^{-7} C/m^{2}K)	p_2	0	-3.5	-6.5	-7.8	-9	-10.8	0
Pyromagnetic constant (10^{-5} C/m^{2}K)	τ_2	0	-36	-28	-23	-18	-8.5	0
Thermal expansion coefficient (10^{-6} K^{-1})	$\alpha_1=\alpha_2$	10	10.8	11.8	12.3	12.9	14.1	15.7
	α_3	10	9.3	8.6	8.2	7.8	7.2	6.4
Density (kg/m^3)	ρ	5400	5500	5550	5600	5700	5800	7750

2.2 Constitutive equations

The constitutive equations for the magneto-electro-elastic (MEE) materials by assuming a linear coupling between elastic, magnetic and electric properties are written as follows

$$\sigma_i = C_{ij}(\varepsilon_j - \alpha_i \Delta T) - e_{ik}E_k - q_{ik}H_k$$

$$D_l = e_{lj}\,\varepsilon_j + \eta_{lk}E_k + m_{lk}H_k + p_k\Delta T \tag{1}$$

$$B_l = q_{lj}\varepsilon_j + m_{lk}E_k + \mu_{lk}H_k + \tau_k\Delta T$$

where i, j =1,2…6 and l, k =1,2,3. In Eq. (1) σ_i, D_l and B_l represents the components of stress, electric displacement and magnetic induction, respectively. C_{ij}, η_{lk} and μ_{lk} are the elastic, dielectric and magnetic permeability constant, respectively. ε_j, E_k, H_k and ΔT are the linear strain tensor, electric field, magnetic field and temperature rise, respectively. Further $e_{lj}, q_{lj}, m_{lk}, \alpha_i, p_k$ and τ_k are the piezoelectric, magnetostrictive, electromagnetic, thermal expansion co-efficient, pyroelectric constant and pyromagnetic constant, respectively. For a transversely isotropic MEE solid, the various material constants appearing in the constitutive Eq. (1) can be represented in the matrix form as follows,

$$[C] = \begin{bmatrix} C_{11} & C_{12} & C_{13} & 0 & 0 & 0 \\ & C_{11} & C_{23} & 0 & 0 & 0 \\ & & C_{33} & 0 & 0 & 0 \\ & & & C_{44} & 0 & 0 \\ & Sym & & & C_{55} & 0 \\ & & & & & C_{66} \end{bmatrix}, [e]^T = \begin{bmatrix} 0 & 0 & 0 & 0 & e_{15} & 0 \\ 0 & 0 & 0 & e_{15} & 0 & 0 \\ e_{13} & e_{13} & e_{33} & 0 & 0 & 0 \end{bmatrix}$$

$$[q]^T = \begin{bmatrix} 0 & 0 & 0 & 0 & q_{15} & 0 \\ 0 & 0 & 0 & q_{15} & 0 & 0 \\ q_{13} & q_{13} & q_{33} & 0 & 0 & 0 \end{bmatrix}, [\mu] = \begin{bmatrix} \mu_{11} & 0 & 0 \\ 0 & \mu_{22} & 0 \\ 0 & 0 & \mu_{33} \end{bmatrix},$$

$$[m] = \begin{bmatrix} m_{11} & 0 & 0 \\ 0 & m_{22} & 0 \\ 0 & 0 & m_{33} \end{bmatrix} \tag{2}$$

$$[\eta] = \begin{bmatrix} \eta_{11} & 0 & 0 \\ 0 & \eta_{22} & 0 \\ 0 & 0 & \eta_{33} \end{bmatrix}, \{\alpha\} = \begin{Bmatrix} \alpha_1 \\ \alpha_2 \\ \alpha_3 \\ 0 \\ 0 \\ 0 \end{Bmatrix}, \{p\} = \begin{Bmatrix} p_1 \\ p_2 \\ p_3 \end{Bmatrix}, \{\tau\} = \begin{Bmatrix} \tau_1 \\ \tau_2 \\ \tau_3 \end{Bmatrix}$$

The strain field related to the displacements can be written as follows

$$\varepsilon_{ij} = \frac{1}{2}\left(u_{i,j} + u_{j,i}\right) \tag{3}$$

The relation between the electric field vector (E) and the electric potential (ϕ) can be represented as

$$E_1 = -\frac{\partial \phi}{\partial x}; E_2 = -\frac{\partial \phi}{\partial y}; E_3 = -\frac{\partial \phi}{\partial z} \tag{4}$$

Similarly, the relation between magnetic field vector (H) and magnetic potential (ψ) is expressed as

$$H_1 = -\frac{\partial \psi}{\partial x}; H_2 = -\frac{\partial \psi}{\partial y}; H_3 = -\frac{\partial \psi}{\partial z} \tag{5}$$

The total potential T_p is given as follows

$$T_p = \frac{1}{2}\int_\Omega \{\varepsilon\}^T \{\sigma\}\, d\Omega - \frac{1}{2}\int_\Omega \{E\}^T \{D\}\, d\Omega - \frac{1}{2}\int_\Omega \{H\}^T \{B\}\, d\Omega - \int_A \{d_t\}^T \{f\}\, dA - \int_A \phi\, Q^\phi dA - \int_A \psi\, Q^\psi dA \tag{6}$$

2.3 Finite element formulation

The discretized FE model of MEE cantilever beam is developed using eight noded 3D brick element. Each node of the element has three degrees of freedom with respect to displacements in x, y and z direction and one degree of freedom corresponding to electric and magnetic potential, respectively. The nodal displacement, electric potential and magnetic potential can be expressed by suitable shape functions as follows

$$u = [N_u]\{u_i\}; \quad \phi = [N_\phi]\{\phi_i\}; \quad \psi = [N_\psi]\{\psi_i\} \tag{7}$$

where, $\{u_i\} = \{u_x, u_v, u_w\}$ are the displacements in x, y and z directions, respectively. N_u, N_ϕ, N_ψ are the shape functions. Further, the strain vector $\{\varepsilon\}$, magnetic field vector $\{H\}$, electric field vector $\{E\}$ are expressed in terms of derivative of shape function matrices as follows

$$\{\varepsilon\} = [B_u]\{d_t^e\}, \quad \{H\} = [B_\psi]\{\psi^e\}, \quad \{E\} = [B_\phi]\{\phi^e\} \tag{8}$$

By substituting Eqs. (1), (7) and (8) in Eq. (6) and assembling the elemental matrices, the coupled finite element equilibrium equations can be written as

$$[K_{uu}]\{u\} + [K_{u\phi}]\{\phi\} + [K_{u\psi}]\{\psi\} = \{F\}_m + \{F_{th}\}$$

$$[K_{u\phi}]^T \{u\} - [K_{\phi\phi}]\{\phi\} - [K_{\phi\psi}]\{\psi\} = \{F_{pe}\} \tag{9}$$

$$[K_{u\psi}]^T \{u\} - [K_{\phi\psi}]^T \{\phi\} - [K_{\psi\psi}]\{\psi\} = \{F_{pm}\}$$

The various elemental stiffness matrices appearing in Eq. (9) are defined by

$$[K_{uu}^e] = \int_V [B_u]^T [C][B_u]\, dV, \quad [K_{u\phi}^e] = \int_V [B_u]^T [e][B_\phi]\, dV, \quad [K_{u\psi}^e] = \int_V [B_u]^T [q][B_\psi]\, dV,$$

$$[K_{\phi\phi}^e] = \int_V [B_\phi]^T [\eta][B_\phi]\, dV, \quad [K_{\phi\psi}^e] = \int_V [B_\phi]^T [m][B_\psi]\, dV, \quad [K_{\psi\psi}^e] = \int_V [B_\psi]^T [\mu][B_\psi]\, dV \tag{10}$$

where, V is the volume of the element. The different shape function derivative matrices appearing in Eq. (10) are given by
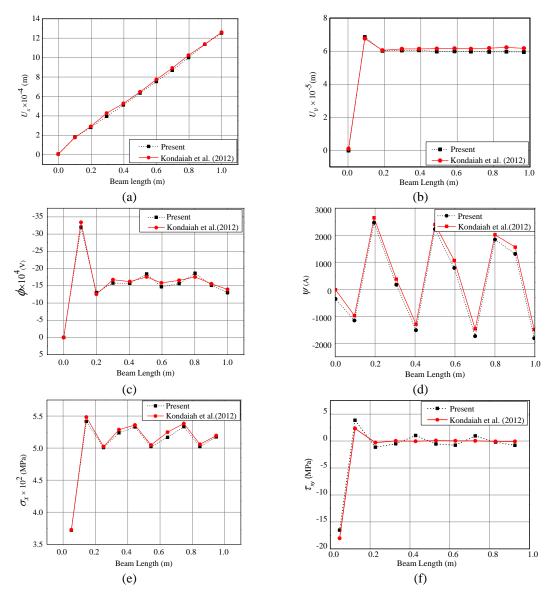
(a)

(b)

(c)

(d)

(e)

(f)

Fig. 2 Validation of (a) longitudinal *x*-direction displacement component (U_x) (b) *y*-direction displacement component (U_v) (c) electric potential (ϕ) (d) magnetic potential (ψ) (f) normal stress - σ_x (f) shear stress - τ_{xy}

$$[B_u] = \begin{bmatrix} \frac{\partial N_1}{\partial x} & 0 & 0 & \frac{\partial N_2}{\partial x} & 0 & 0 & & \frac{\partial N_8}{\partial x} & 0 & 0 \\ 0 & \frac{\partial N_1}{\partial y} & 0 & 0 & \frac{\partial n_2}{\partial y} & 0 & & 0 & \frac{\partial N_8}{\partial y} & 0 \\ 0 & 0 & \frac{\partial N_1}{\partial z} & 0 & 0 & \frac{\partial N_2}{\partial z} & \cdots\cdots & 0 & 0 & \frac{\partial N_8}{\partial z} \\ 0 & \frac{\partial N_1}{\partial z} & \frac{\partial N_1}{\partial y} & 0 & \frac{\partial N_2}{\partial z} & \frac{\partial N_2}{\partial y} & & 0 & \frac{\partial N_8}{\partial z} & \frac{\partial N_8}{\partial y} \\ \frac{\partial N_1}{\partial z} & 0 & \frac{\partial N_1}{\partial x} & \frac{\partial N_2}{\partial z} & 0 & \frac{\partial N_2}{\partial x} & & \frac{\partial N_8}{\partial z} & 0 & \frac{\partial N_8}{\partial x} \\ \frac{\partial N_1}{\partial y} & \frac{\partial N_1}{\partial x} & 0 & \frac{\partial N_2}{\partial y} & \frac{\partial N_2}{\partial x} & 0 & & \frac{\partial N_8}{\partial y} & \frac{\partial N_8}{\partial x} & 0 \end{bmatrix}; \quad [B_\psi] = \begin{bmatrix} \frac{-\partial N_1}{\partial x} & \frac{-\partial N_2}{\partial x} & \frac{-\partial N_8}{\partial x} \\ -\frac{\partial N_1}{\partial y} & -\frac{\partial N_2}{\partial y} \cdots & -\frac{\partial N_8}{\partial y} \\ -\frac{\partial N_1}{\partial z} & -\frac{\partial N_2}{\partial z} & -\frac{\partial N_8}{\partial z} \end{bmatrix}; \quad [B_\phi] = [B_\psi] \tag{11}$$
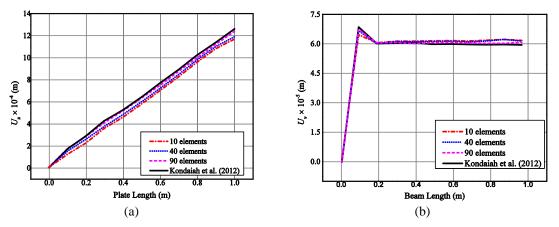
Fig. 3 Convergence of (a) longitudinal *x*-direction (U_x) (b) *y*-direction displacement component

Further, the different load vectors $\{F_m\}$, $\{F_{th}\}$, $\{F_{pe}\}$ and $\{F_{pm}\}$ are the mechanical, thermal, pyroelectric and pyromagnetic load vectos, respectively. They are represented as follows

$$\left\{F_m^e\right\} = \int_A \left[N_t\right]^T f \, dA, \quad \left\{F_{th}^e\right\} = \int_V \left[B_t\right]^T \left[C\right]\{\alpha\}\Delta T dV, \quad \left\{F_{pe}^e\right\} = \int_V \left[B_\phi\right]^T \left[p\right]\Delta T dV, \quad \left\{F_{pm}^e\right\} = \int_V \left[B_\psi\right]^T \left[\tau\right]\Delta T dV \quad (12)$$

where, f is the traction force acting on the plate surface A. By eliminating the electric and magnetic potential terms in Eq. (8), the equivalent stiffness matrix $[K_{eq}]$ is derived to obtain the nodal displacements.

$$[K_{eq}]\{u\} = \{F_{eq}\} \quad (13)$$

3. Results and discussion

The finite element formulation derived in the preceding section is initially solved for validation and comparison with the existing results. The numerical illustrations are presented to analyse the behavior of MEE cantilever beam subjected to thermo-mechanical load. The dimensions of the beam geometry considered for analysis can be described as follows: the length of the beam L is 1 m, width w=0.1 m and the thickness h=0.1 m. In this case, the loading condition refers to the combined effect of the uniform temperature rise of 10 K and sinusoidaly varying mechanical load $q = q_o \sin \pi x/l$ with the amplitude $q_0 = 1.5 \, kN/m$. The material properties corresponding to volume fraction (V_f) 50% BaTiO$_3$, given in Table 1 is used, unless and otherwise stated. Also, a comparative study of the individual effect of the thermal and mechanical load with the combined thermo-mechanical load is discussed. The influence of the pyroelectric and pyromagnetic effects is considered. The study also attempts to evaluate the effect of the volume fraction and various types of mechanical loads on the static parameters of MEE cantilever beam.

3.1 Validation of the finite element formulation

For the purpose of validation, the results presented by Kondaiah *et al.* (2012) for purely thermal
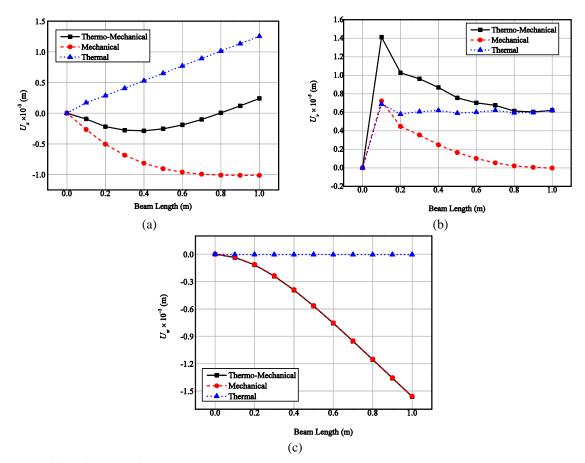
Fig. 4 Effect of loading forms on the (a) longitudinal *x*-direction (U_x) (b) *y*-direction (U_v) (c) transverse *z*-direction (U_w) displacement components

MEE beam is reproduced using the present finite element formulation. In this regard the effect of mechanical load is nullified in the formulation. Further, the loading form, boundary conditions and beam geometry are adopted similar to Kondaiah *et al.* (2012). The material properties corresponding to the various volume fractions of $BaTiO_3$ and $CoFe_2O_4$ are tabulated in Table 1. The validation plots for longitudinal *x*-direction (U_x), *y*-direction (U_v), electric potential (ϕ), magnetic potential (ψ), normal stress (σ_x) and shear stress (τ_{xy}) are illustrated in Figs. 2(a)-(f), respectively. From these figures it is witnessed that the results from the present FE formulation are in good agreement with each other. Hence, it can be justified that the finite element formulation and MATLAB code generated can faithfully produce the results. In addition, the convergence rate of the solution obtained from the present FE formulation with respect to various mesh densities are illustrated in Figs. 3(a) and (b), considering the displacement components U_x and U_v.

3.2 Comparative study of the thermal, mechanical and thermo-mechanical loadings

In this section, the influence of combined effect of thermal and mechanical loads on the static behaviour of MEE beam is analysed. The numerical analysis reveals that the longitudinal *x*-
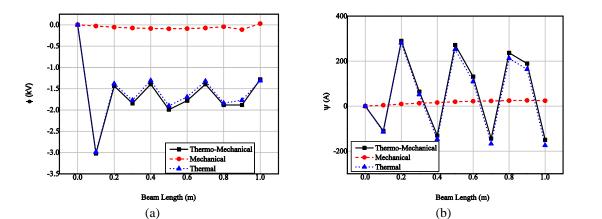
(a)   (b)

Fig. 5 Effect of loading forms on the (a) electric potential (ϕ) (b) magnetic potential (ψ)

(a)   (b)

(c)

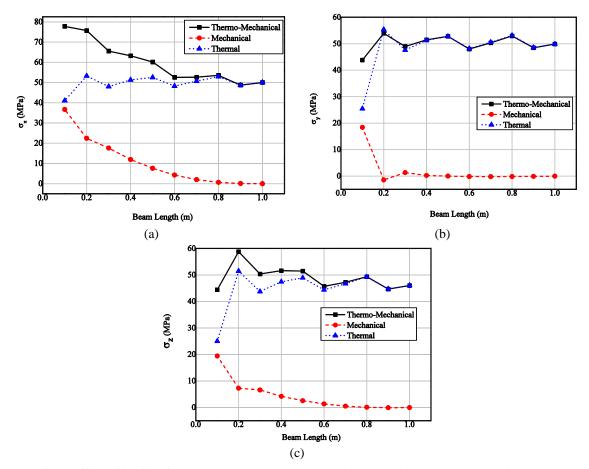Fig. 6 Effect of loading forms on the (a) normal stress-σ_x (b) normal stress-σ_y (c) normal stress-σ_z

direction displacement component U_x is more when MEE beam is subjected to thermal loading alone, as shown in Fig. 4(a). Considering Fig. 4(b), it may be noticed that the combination of
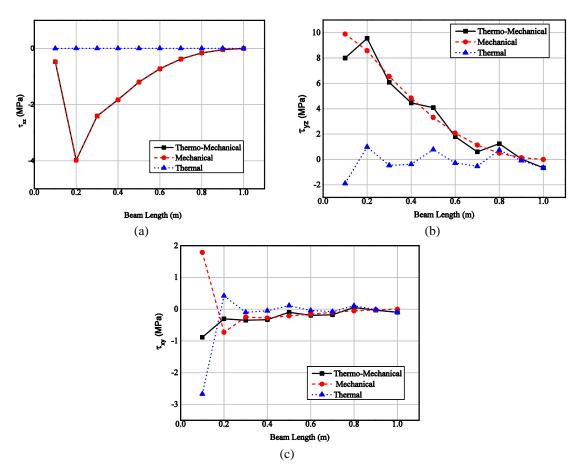
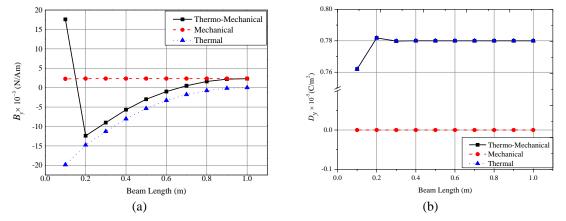Fig. 7 Effect of loading forms on the (a) shear stress-τ_{xz} (b) shear stress-τ_{yz} (c) shear stress-τ_{xy}

Fig. 8 Effect of loading forms on the (a) magnetic flux density-B_y (b) electric displacement-D_y

thermal and mechanical loads have a predominant effect on U_v while, the mechanical load alone has comparatively lesser effect. Fig. 4(c) elucidates the distribution of transverse z-direction

Fig. 9 Effect of volume fraction on the (a) longitudinal *x*-direction (U_x) (b) *y*-direction (U_v) (c) transverse *z*-direction (U_w) displacement components (d) electric potential (ϕ) (e) magnetic potential (ψ)

displacement component U_w along the beam length. It can be noticed that in contrast with the thermo-mechanical and mechanical loading, individual effect of thermal load is least significant.
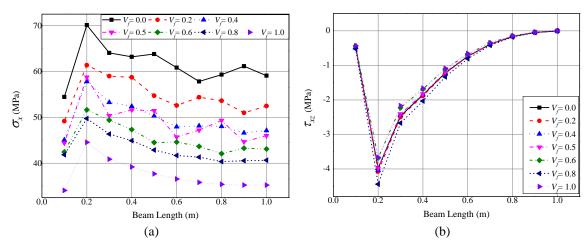
Fig. 10 Effect of volume fraction on the (a) normal stress (σ_x) (b) shear stress-τ_{xz}

Fig. 5(a) illustrates the variation of the electric potential (ϕ) under different loading conditions. The substantial effect of the thermal load can be noticed whereas, the influence of the mechanical load is found to be insignificant. The similar characteristic behaviour is observed for the magnetic potential also as elucidated in Fig. 5(b).

The variations of normal stresses σ_x, σ_y and σ_z are depicted in Figs. 6(a)-(c), respectively. It can be observed that MEE beam experiences the maximum normal stresses when the combined effect of the thermal and mechanical load is considered. Also it can be witnessed that the mechanical load has a least influence on the normal stresses.

Further, the thermal loading produces insignificant amount of shear stress τ_{xz}, as plotted in Fig. 7(a). The numerical evaluation also suggests that the maximum stress is observed near the clamped end. The thermo-mechanical and individual mechanical load results in an almost similar variation of τ_{yz} as shown in Fig. 7(b). Furthermore, along the beam length a negligible discrepancy is noticed for τ_{xy} among the three loading forms as displayed in Fig. 7(c).

The effect of thermo-mechanical loads and individual thermal and mechanical loads on y-direction magnetic flux density component (B_y) and electric displacement component (D_y) is shown in Figs. 8(a) and (b) respectively. It can be observed that for both the components, mechanical loading has a negligible effect.

3.3 Effect of volume fraction

The numerical evaluation is extended to compute the influence of volume fraction (V_f) on the direct and derived quantities of MEE cantilever beam under thermo-mechanical loading. From the results plotted in Figs. 9(a)-(e), it may be observed that the maximum value of displacement components U_x and U_w are witnessed for V_f=1.0. This may be due to lesser stiffness of MEE beam corresponding to pure piezoelectric phase (V_f=1.0), which allows greater deformation of MEE beam. Meanwhile, U_v is found to be maximum for the volume fraction corresponding to 0.8. Further, the maximum electric potential (ϕ) is observed for pure piezoelectric phase (V_f=1.0) whereas, the maximum magnetic potential (ψ) is observed for V_f=0.5.

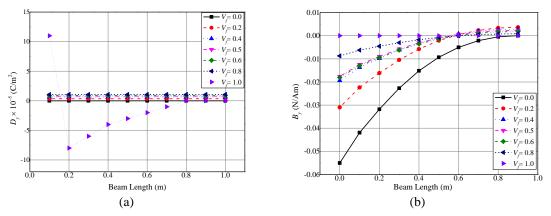The variations of normal stress σ_x and shear stress τ_{xz} is illustrated in Figs. 10(a) and (b),

Fig. 11 Effect of volume fraction on the (a) magnetic flux density-B_y (b) electric displacement-D_y

respectively. It suggests that $V_f=0.0$ results in a higher normal stress σ_x while, $V_f=0.8$ influences the shear stress τ_{xz} to a greater extent.

The $V_f=1.0$ has a significant effect on the electric displacement component (D_y) as shown in Fig. 11(a). This may be due to higher piezoelectric coefficients which directly affects the electric displacement. Also, from Fig. 11(b), the maximum magnetic flux density (B_y) is observed for $V_f=0.0$.

3.4 Effect of different types of mechanical loading

The numerical evaluation is extended to analyse the effect of different mechanical loading profiles acting on MEE cantilever beam along with the uniform temperature rise of 10 *K*. The material properties of $V_f=0.5$ BaTiO$_3$ is used. The different forms of mechanical loading considered for the present analysis are as follows:

3.4.1 Sinusoidal loading
The mechanical load is assumed to vary sinusoidally along the beam length with the general equation $q = q_o \sin \pi x/l$ with the amplitude $q_0 = 1.5 \, kN/m$, *l* is the beam length and *x* is the distance of the point of interest from the clamped end.

3.4.2 Uniformly distributed load (UDL)
In this case, the mechanical load is uniformly distributed throughout the beam length *l*. It can be represented by the general equation $q=q_o$.

3.4.3 Point load
The point load of 1.5 kN is acted on the free end of the cantilever MEE beam along the negative *z*-direction.

The numerical evaluation suggests that for a MEE beam, along with temperature rise of 10 K, the UDL mechanical load produces maximum displacement components U_x, U_v and U_w as plotted in Figs. 12(a)-(c). Also, it is witnessed from Figs. 12(d)-(e) that the various mechanical load forms considered displays an insignificant effect on the variation of electric and magnetic potentials of the beam.
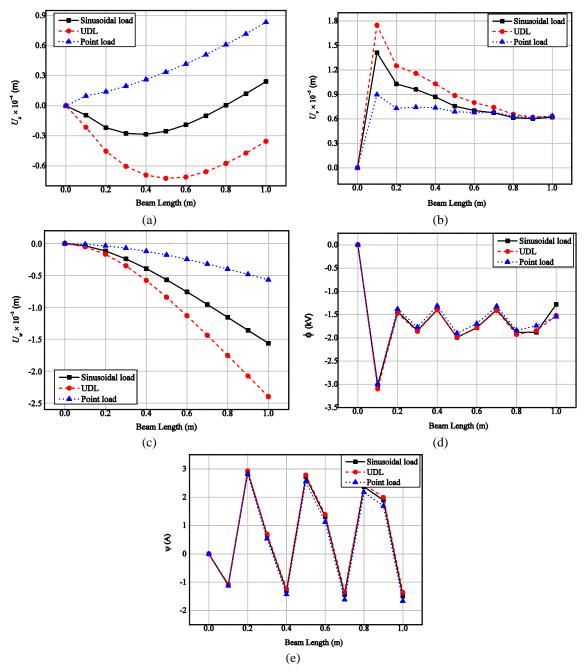
Fig. 12 Effect of types of mechanical loads on (a) longitudinal *x*-direction (U_x) (b) *y*-direction (U_v) (c) transverse *z*-direction (U_w) displacement components (d) electric potential (ϕ) (e) magnetic potential (ψ)

The variations of the stresses are shown in Figs. 13(a)-(f). The significant effect of the UDL on the stresses may be observed. It may be attributed to the constant load distribution through the beam length. Further, in contrast with the sinusoidal and UDL loads, the point load has the least effect on the stresses.

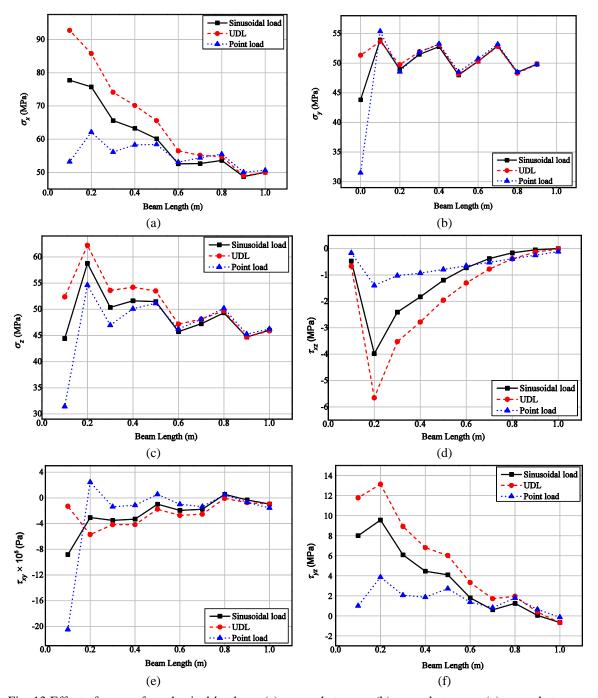Fig. 13 Effect of types of mechanical loads on (a) normal stress-σ_x (b) normal stress-σ_y (c) normal stress-σ_z (d) shear stress-τ_{xz} (e) shear stress-τ_{xy} (f) shear stress-τ_{yz}

Figs. 14(a) and (b) display the variation of electric displacement and magnetic flux density, respectively. It is worth mentioning that no discrepancies can be noticed among all the three forms
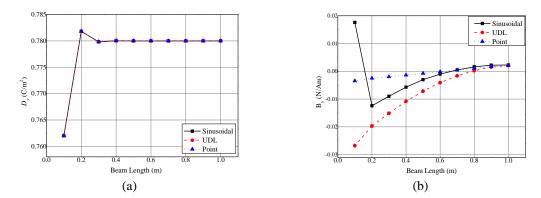
Fig. 14 Effect of types of mechanical loads on (a) electric displacement component-D_y (b) magnetic flux density component-B_y

of mechanical loads with respect to electric displacement D_y while, the UDL has a predominant effect on B_y. In addition, maximum B_y is experienced at the clamped end which reaches to zero at the free end whereas, D_y varies constantly along the beam length.

4. Conclusions

In the present work, the static behaviour of a multiphase magneto-electro-elastic (MEE) cantilever beam subjected to thermo-mechanical loading is analysed using finite element (FE) methods. The 3D formulation developed can represent more realistic geometric refinements and thus they are highly reliable. Incorporating the 3D solid elements in the FE model assures the representation of the physical system accurately. Further, the convergence study carried out suggests that an optimum mesh density has been selected for the FE analysis. The evaluation of the MEE beam is made in terms of the displacement components, potentials and stresses, varying along the beam length. Also, a comparative study of the influence of thermo-mechanical loads is made with the individual effects of thermal and mechanical loads. The numerical evaluation suggests that the electric and magnetic potential of the system is predominantly influenced by the thermal loads, whereas mechanical loads have a minimal contribution. The reason may be perhaps because of the additional thermo-electric and thermo-magnetic coupling developed due to thermal loads. Further, the combined effect of thermal and mechanical load result in the increased stresses of MEE beam. The pure piezoelectric phase results in higher displacement components which are attributed to the lower values of elastic stiffness coefficients. Also, maximum electric displacement and magnetic flux density is witnessed for pure piezoelectric and pure piezomagnetic phases, respectively. Among the various mechanical load forms considered, uniformly distributed mechanical load along with the uniform temperature rise is observed to have a dominant effect on the static behaviour of the MEE cantilever beam. Further, an insignificant effect of the load profiles on the potentials and electric displacement of MEE beam is noticed. It is believed that the results from the present analysis assist in precise designing of sensors in thermo-mechanical environment.

References

Annigeri, A.R., Ganesan, N. and Swarnamani, S. (2007), "Free vibration behavior of multiphase and layered magneto-electro-elastic beam", *J. Sound Vibr.*, **299**(1-2), 44-63.

Ansari, R., Gholami, R. and Rouhi, H. (2015), "Size-dependent nonlinear forced vibration analysis of magneto-electro-thermo-elastic Timoshenko nanobeams based upon the nonlocal elasticity theory", *Compos. Struct.*, **126**, 216-226.

Biju, B., Ganesan, N. and Shankar, K. (2012), "Effect of displacement current in magneto–electro-elastic plates subjected to dynamic loading", *J. Mech. Mater. Des.*, **8**, 349-358.

Biju, B., Ganesan, N. and Shankar, K. (2012), "Transient dynamic behaviour of two phase magneto-electro-elastic sensors bonded to elastic rectangular plates", *J. Smart Sens. Intell. Syst.*, **5**(3).

Farzad, E. and Mohammad, R.B. (2016), "Dynamic modeling of a thermo-piezo-electrically actuated nanosize beam subjected to a magnetic field", *Appl. Phys.-A*, **122**, 451.

Jandaghian, A.A. and Rahmani, O. (2016), "Free vibration analysis of magneto-electro thermo-elastic nanobeams resting on a Pasternak foundation", *Smart Mater. Struct.*, **25**, 035023.

Kattimani, S.C. and Ray, M.C. (2014), "Active control of large amplitude vibrations of smart magneto-electro-elastic doubly curved shells", *J. Mech. Mater. Des.*, **10**(4), 351-378.

Kattimani, S.C. and Ray, M.C. (2014), "Smart damping of geometrically nonlinear vibrations of magneto-electro-elastic plates", *Compos. Struct.*, **14**, 51-63.

Kattimani, S.C. and Ray, M.C. (2015), "Control of geometrically nonlinear vibrations of functionally graded magneto-electro-elastic plates", *J. Mech. Sci.*, **99**, 154-167.

Kim, J.Y., Li, Z. and Baltazar, A. (2012), "Pyroelectric and pyromagnetic coefficients of functionally graded multilayered multiferroic composites", *Acta Mech.*, **223**, 849-860.

Kondaiah, P., Shankar, K. and Ganesan, N. (2012), "Studies on magneto-electro-elastic cantilever beam under thermal environment", *Coupled Syst. Mech.*, **1**(2), 205-217.

Kondaiah, P., Shankar, K. and Ganesan, N. (2013), "Pyroelectric and pyromagnetic effects on behavior of magneto-electro-elastic plate", *Coupled Syst. Mech.*, **2**, 1-22.

Kumaravel, A., Ganesan, N. and Sethuraman, R. (2007), "Steady-state analysis of a three-layered electro-magneto-elastic strip in a thermal environment", *Smart Mater. Struct.*, **16**(2), 282-295.

Milazzo, A (2013), "A one-dimensional model for dynamic analysis of generally layered magneto-electro-elastic beams", *J. Sound Vibr.*, **332**(2), 465-483.

Pan, E. and Han, F. (2005), "Exact solution for functionally graded and layered magneto-electro-elastic plates", *J. Eng. Sci.*, **43**(3-4), 321-339.

Rajesh, K., Bhangale, G.N. (2006), "Free vibration of simply supported functionally graded and layered magneto-electro-elastic plates by finite element method", *J. Sound Vibr.*, **294**, 1016-1038.

Sunar, M., Ahmed, Z., Al-Garni, A.M.H. and Kahraman, R. (2002), "Finite element modeling of thermopiezomagnetic smart structures", *AIAA J.*, **40**(9), 1846-1851.

Thar, M.B. and Hussain, H.A.K. (2013), "Analytical solution for simply supported and multilayered magneto-electro-elastic plates", *Asian J. Sci. Res.*, **6**, 236-244.

Vaezi, M., Shirbani, M.M. and Hajnayeb, A. (2016), "Free vibration analysis of magneto-electro-elastic microbeams subjected to magneto-electric loads", *Phys. E: Low-Dimens. Syst. Nanostruct.*, **75**, 280-286.

Vinyas, M. and Kattimani, S.C. (2017a), "Static studies of stepped functionally graded magneto-electro-elastic beam subjected to different thermal loads", *Compos. Struct.*, **163**, 216-237.

Vinyas, M. and Kattimani, S.C. (2017b), "Static analysis of stepped functionally graded magneto-electro-elastic plates in thermal environment: A finite element study", *Compos. Struct.*

Vinyas, M. and Kattimani, S.C. (2017c), "A Finite element based assessment of static behavior of multiphase magneto-electro-elastic beams under different thermal loading", *Struct. Eng. Mech.*, **62**(5), 519-535.

Yoshihiro, O. and Yoshinobu, T. (2005), "Transient analysis of multilayered magneto-electro-thermoelastic strip due to nonuniform heat supply", *Compos. Struct.*, **68**, 471-480.

CC